Effect of Proton Irradiation on the Corrosion Behaviors of Ferritic/Martensitic Steel in Liquid Metal Environment

Jeonghyeon Lee[a], Tae Yong Kim[a], and Ji Hyun Kim[a*]

[a] *School of Mechanical and Nuclear Engineering, Ulsan National Institute of Science and Technology (UNIST), Ulju-gun, Ulsan 44919, Republic of Korea*
[*]Corresponding author: kimjh@unist.ac.kr

1. Introduction

Liquid metal fast breeder reactors (LMFBRs) such as sodium-cooled fast reactor (SFR) and lead-cooled fast reactor (LFR) are the candidates of GEN-IV nuclear energy systems. Among various liquid metals that can be used as primary coolant material, sodium is a world widely used coolant for GEN-IV reactors [1]. As a coolant for fast reactor systems, liquid sodium provides some advantages over liquid lead or lead-bismuth eutectic (LBE). Sodium is a more effective heat transfer medium than water about 100 times and it has a wide temperature margin about 400 ℃ to boil. Sodium has not only a reasonably low melting point but also a low boiling point (883 ℃). This property raises safety concerns regarding the unprotected transients which lead to a coolant heatup. And the velocity of LBE or lead coolant is limited to about 2.5-3.0 m/s by erosion concerns for protective oxide layers. Typical velocities of sodium are up to 8–10 m/s, hence lead has a lower heat removal capacity, in practice. These make it possible to lead a higher linear power and to require a lower pitch to diameter ratio [2,3].

Gr.92 (ferritic/martensitic steel, FMS) is considered as a candidate of cladding material for sodium-cooled fast reactors (SFRs).

Its compatibility with sodium is the one of issues, especially in point of dissolution, chemical reaction, and carbon transfer with impurities which degrade the mechanical properties. Therefore, the compatibility of cladding and structural materials with sodium has to be carefully investigated.

Sodium can promote corrosion of cladding and structural materials in two ways. One is a dissolution of alloy constituents into the sodium, and the other is a chemical reaction with impurities (especially oxygen and carbon) in the sodium environment [4].

In ultra-long cycle fast reactor (UCFR) which is developed by UNIST, cladding is exposed for a long-term in high temperature liquid sodium environment [5]. So, it is very important to investigate the corrosion-related behavior such as surface corrosion rate, carburization, decarburization and mechanical properties change during operation period.

Decarburization means dissolved carbon diffusion from the specimen surface into the liquid sodium. This process can originate from the different activity of dissolved carbon between the material and liquid sodium. Compatibility test of the cladding tube revealed that aging caused a decrease of mechanical properties, and it governed the whole mechanical properties [6].

The structural materials exposed to the liquid sodium for a long time experience highly corrosive environments. High temperature may reduce the margin of safety against failure during normal operation and may promote corrosion [7–9].

During operation of nuclear power plant, the cladding material will face neutron and multiple types of ion beam irradiation, which can induce structural damage of the cladding [10–12]. Proton irradiation has been used in the past decades to reproduce neutron damage since proton has a higher scattering cross-section than fast neutron. So it leads to a displacement rate for nuclear material research [13–15]. Besides, reduction of total elongation linearly increases as dose increases, and the dose increment significantly influences tensile properties of liquid metal [16].

In this study, FMS and irradiated FMS were tested in point of corrosion and dissolution. The combined effect of irradiation and liquid metal corrosion on the FMS is concluded. Especially, how irradiation conditions affect corrosion rate of the steels in liquid metal environment was conducted.

2. Experimental

The composition of the Gr.92 and HT9 used in this experiment is given in Table 1. Heat treatment such as normalizing and tempering was performed. The both specimens were normalized at 1050 ℃ for 1 hour followed by air cooling, and then they were tempered at 780 ℃ for 30 min. Each sample was cut into small strip with size: 10mm×5mm×2mm and polished successively with 320, 400, 600, and 800 grit emery paper and diamond polishing up to 1 μm. It was cleaned by

ultrasonic cleanser with ethanol, acetone, and distilled water in sequence.

Table 1. Chemical composition of the test material (wt.%)

	C	Si	Mn	Cr	Ni	Mo	W	V
Gr.92	0.087	0.21	0.41	8.69	0.13	0.38	1.62	0.18
HT9	0.19	0.14	0.49	12.05	0.48	1.00	0.49	0.30

The proton irradiation experiments were carried out in TR23 (20 MeV) accelerator from KOMAC (Korea multi-purpose accelerator complex), gyeong-ju, Korea. The beam dump of KOMAC is located the photon production downstream are for a continuous absorption of the generated beam energy [17].

In the case of irradiation with 3 MeV protons, the proton fluences were 5×10^{15} #/cm^2 and 1×10^{16} #/cm^2, respectively. Those fluences were the maximum terms for highest displacement per atom at KOMAC. The stability of the current was within ±5 %. The largest average current is 0.6 mA, pulse width is 0.05 ms. The total damage and depth of stopping range of the sample were calculated through the stopping and range of ions in matter code (SRIM).

The immersion experiment was performed in the glove box in order to examine the effectiveness of irradiation and chrome concentration in specimen as a function of the exposure time. The experimental setup, shown in Fig. 1, had the capability for safety sodium immersion experiment under high temperature and long exposure time. Dissolved oxygen was also saturated in the liquid sodium. Each specimen was taken out after 100 h, 200 h and 300 h, respectively.
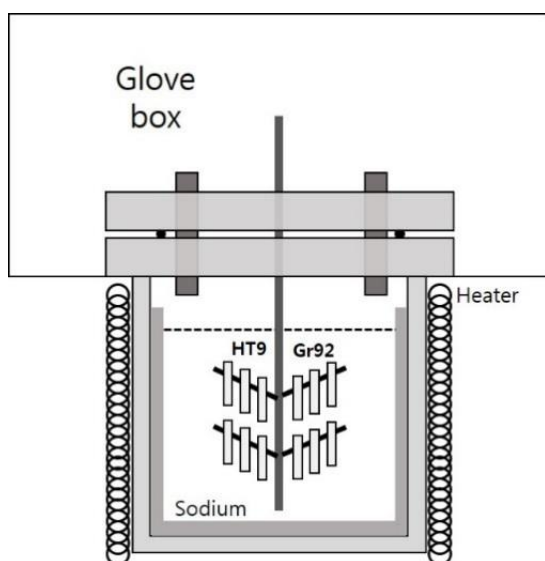
Fig. 1. Schematic of liquid sodium experimental facility,

3. Results and Discussion

The proton irradiation experiment and immersion experiments were conducted for this study at two different dose rate conditions and various exposure time.

3.1 Irradiation result

Irradiations were conducted by using 3 MeV protons, which have a penetration distance about 40 μm in stainless steel, to prevent implantation within the 30 μm sample. An example of the hydrogen profile and dpa profile calculated by the SRIM is shown in the below graph. The damage profile of SRIM simulation is illustrated in Fig. 2. The damage profile was fairly flat at an average of 3×10^{-5} displacements/angstrom-ion. From the SRIM result, it can be verified that the irradiated specimen can be used to immersion test.
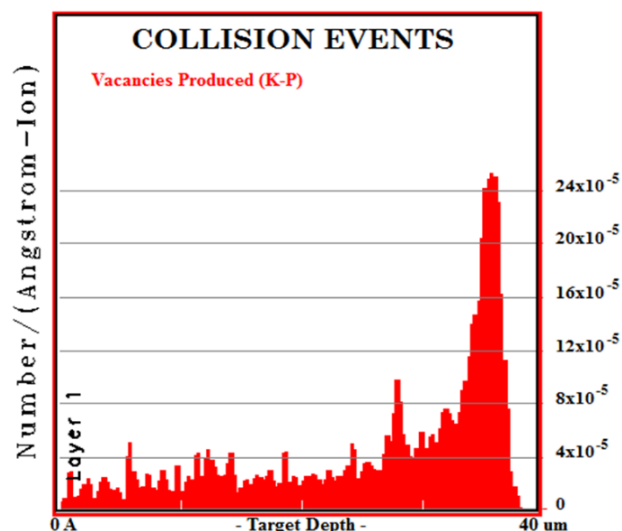
Fig. 2. SRIM result of 3MeV proton beam incident on Gr.92 target. Damage peak occurs around 38 μm of the sample. Nominal sample thickness of 30 μm was used to avoid the damage peak and any proton implantation,

3.2 Immersion test

Oxygen dissolves in sodium as the monoxide Na_2O. By this formation, we may assume the reaction (Equation (1)). In the liquid sodium environment, $NaCrO_2$ is more stable than Na_2O [9]. Na_2O encounters electrons, then it forms NaO_2^{3-} and Na (Equation (2)). And chrome atom emits the electron which is cation (Equation (3)).

And chromium is a strong oxide former, and sodium chromite, $NaCrO_2$, forms readily according to the

reaction (Equation (4)). The reaction has been written for Na_2O in solution in sodium.

$$2\text{Na(l)} + \frac{1}{2}O_2 \rightarrow Na_2O(s) \qquad (1)$$

$$2Na_2O(s) + 3e \rightarrow NaO_2^{3-} + 3Na(l) \qquad (2)$$

$$Cr(s) \rightarrow Cr^{3+} + 3e \qquad (3)$$

$$2\text{Na}_2O(soln) + Cr(s) \rightarrow NaCrO_2 + 3Na(l) \qquad (4)$$
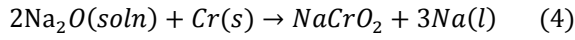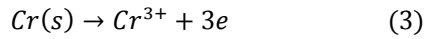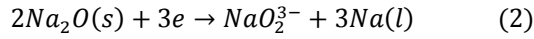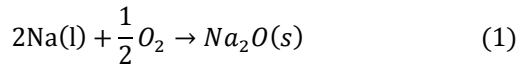
The immersion tests at higher temperature with as-received and irradiated HT9 and Gr.92 specimens are under process and also as-received specimens were exposed to oxygen saturated sodium environment to form $NaCrO_2$ on the surface

To explain the existence of $NaCrO_2$, EDS analysis is performed with X-ray mapping analysis and point analysis. In order to confirm the existence of $NaCrO_2$, X-ray photoelectron spectroscopy (XPS) analysis was also performed with same specimens. Result shows that XPS spectra of the specimen after 300 h at 650 ℃ oxygen-saturated sodium including survey, C_{1s}, O_{1s}, Na_{1s}, and Cr_{2p} spectra, and the result confirms the existence of $NaCrO_2$ compound in the surface of specimen.

Fig. 3 shows the FIB images of the as-received, 0.006 dpa, and 0.012 dpa specimens. Dark regions indicate chromium-rich zones, which are ~9.98 μm, ~11.64 μm, and 12.32 μm thick, respectively. The thicknesses of the chromium-rich zones on the as-received specimens are more thin than that of the irradiated specimen. The chromium-rich zone on the as-received specimen is the thinnest because the specimen damage is relatively small.

(a)

(b)

(c)
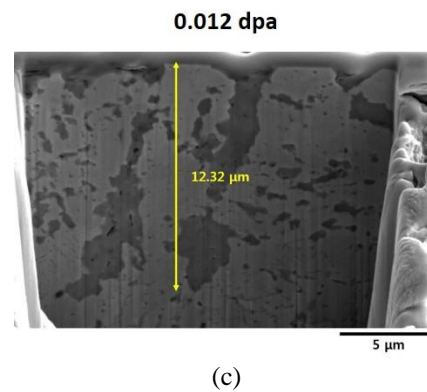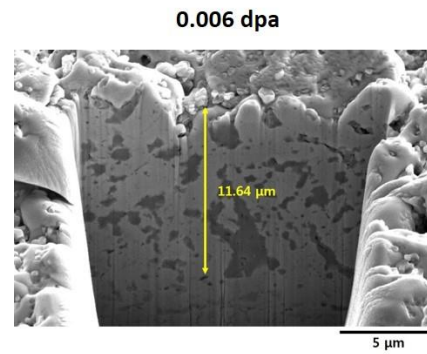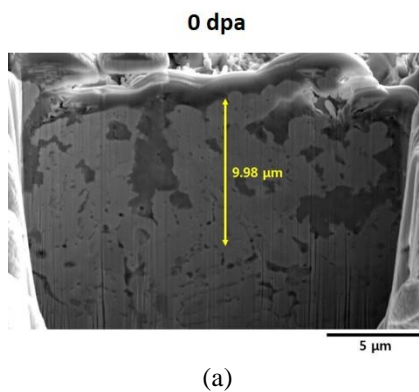
Fig. 3. FIB-SEM images of (a) as-received, (b) 0.006 dpa damaged specimen, and (c) 0.012 dpa damaged specimen after 300 h exposure in 650 ℃ oxygen-saturated sodium. The vertical arrow bars indicate the thickness of chromium rich zone from the surface of the metal.

3.3 Factor of corrosion acceleration

Fig. 4 shows the atomic forced microscopy (AFM) photographs of surface morphology of specimen before and after H+ ion irradiation. It could be observed from the figure that, after irradiation, both the surface projections and the rms roughness of specimen increased. The evolution of ion beam irradiated solid surface was the result of a competition between the roughening process caused by ion bombardment and the smoothing process caused by material transport. It was clear that the roughening process caused by ion bombardment played a dominant role [18]. These results indicate that the grain matrices were also heavily attacked by the sodium, and hence proton ion irradiation significantly increases intergranular corrosion in the irradiated and corroded sample. Moreover, a large number of small cavities and $NaCrO_2$ were observed on the surface.
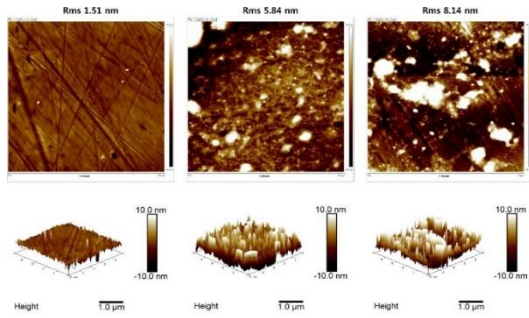
Fig. 4. AFM micrographs showing the change in surface morphology for specimen irradiated by protons with various fluences.
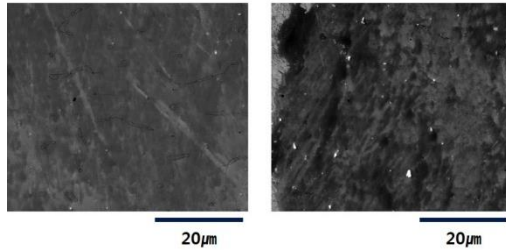
Fig. 5. SEM observation of the Cr-rich phase in the specimen irradiated

Enrichment or depletion of solute in sink such as grain boundary, irradiation can form precipitate directly if the local solute concentration exceeds solubility limit. Therefore, the precipitation of the materials under irradiation can be an example of radiation-induced precipitation in an undersaturated solid solution. Depending on the amount of proton irradiation, radiation induced precipitation can increase in the irradiated materials. Fig. 5 shows this phenomenon.

4. Conclusions

In this study, as-received Gr.92 and irradiated Gr.92 specimen in the oxygen-saturated liquid sodium were examined at high temperature for 300h. The microstructure results reveal the information of the effect of irradiation and effect of the chrome concentration in specimen.

i. From the SRIM result, penetration distance of 40 μm in stainless steel and nominal sample thickness of 30 μm was used to avoid the damage peak and any proton implantation

ii. From the microstructural evaluation, chromium-rich zones existed under the surface of the both of non-irradiated and irradiated materials. The irradiated materials showed chromium-rich zones with larger depths than the non-irradiated specimens**.**

iii. Through the weight loss measurement, it was observed that materials, which has the reduced chromium content by proton irradiation, loses its weight relatively more.

iv. Corrosion resistance was degraded with (a) the increased of surface roughness, (b) chromium depletion by radiation induced precipitation, and (c) potential path for corrosion by radiation defect, which are caused by irradiation.

ACKNOWLEDGEMENTS

REFERENCES

[1] S.H. Shin, S.H. Kim, J.H. Kim, J. Nucl. Mater. 450 (2014) 314.
[2] J. Carlsson, H. Wider, Comparison of sodium and lead-cooled fast reactors regarding reactor physics aspects , severe safety and economical issues, 236 (2006) 1589.
[3] P. Mazgaj, P. Darnowski, S. Gurgacz, M. Lipka, K. Dziubanii, Comparison of Simple Design of Sodium and Lead Cooled Fast Reactor Cores, 94 (2014) 16.
[4] T. Furukawa, S. Kato, E. Yoshida, J. Nucl. Mater. 392 (2009) 249.
[5] J.A. Jung, S.H. Kim, S.H. Shin, I.C. Bang, J.H. Kim, J. Nucl. Mater. 440 (2013) 596
[6] J.H. Kim, S.H. Kim, J. Nucl. Mater. 443 (2013) 112
[7] M.C. Billone, T. a. Burtseva, R.E. Einziger, J. Nucl. Mater. 433 (2013) 431
[8] S.H. Shin, J.H. Lee, J.K. Lee, J. Lim, S. Choi, G. Kim, J.H. Kim, J. Electrochem. Soc. 162 (2015) B152
[9] J. Lee, S.H. Shin, J.K. Lee, S. Choi, J.H. Kim, J. Power Sources. 307 (2016) 526
[10] W.J.S. Yang, J. Nucl. Mater. 158 (1988) 71
[11] G.E. Lucas, M. Surprenant, J. Dimarzo, G.J. Brown, J. Nucl. Mater. 101 (1981) 78
[12] J.J. Kai, W.I. Huang, H.Y. Chou, J. Nucl. Mater. 170 (1990) 193
[13] H.H. Shen, S.M. Peng, X. Xiang, F.N. Naab, K. Sun, X.T. Zu, J. Nucl. Mater. 452 (2014) 335
[14] L. Tournadre, F. Onimus, J.L. B. chade, D. Gilbon, J.M. Clou, J.P. Mardon, X. Feaugas, O. Toader, C. Bachelet, J. Nucl. Mater. 425 (2012) 76
[15] L. Tournadre, F. Onimus, J.L. Béchade, D. Gilbon, J.M. Cloué, J.P. Mardon, X. Feaugas, J. Nucl. Mater. 441 (2013) 222
[16] E. Stergar, M. Lambrecht, S. Gavrilov, TWIN-ASTIR irradiation programs, 468 (2016) 228
[17] J. Kim, C.S. Gil, W. Maeng, D. Kim, Nucl. Instruments Methods Phys. Res. Sect. A Accel. Spectrometers, Detect. Assoc. Equip. 562 (2006) 997
[18] H. Zhang, X. Mei, Y. Wang, Z. Wang, Y. Wang, J. Nucl. Mater. 456 (2015) 344